Structural characterization of a high-temperature, ionic conducting ceramic using perturbed angular correlation spectroscopy

Gary L. Catchen, Lorenz H. Menke, Jr., Michael Blaszkiewicz, and Khalid Jamil
Center for Electronic Materials and Devices and Department of Nuclear Engineering, The Pennsylvania State University, University Park, Pennsylvania 16802

Dinesh K. Agrawal, Wayne Huebner, and Herbert A. McKinstry
Materials Research Laboratory, The Pennsylvania State University, University Park, Pennsylvania 16802
(Received 10 July 1987; revised manuscript received 9 October 1987)

Perturbed angular correlation (PAC) spectroscopy has been used to characterize several structural aspects of a high-temperature, ionic conducting ceramic, $CaZr_{3.95}Hf_{0.05}P_6O_{24}$. Hafnium was introduced into the material to provide the PAC probe nuclei, $^{181}Hf/^{181}Ta$, which were located primarily at Zr sites. PAC measurements were made over a range of temperatures from 77 to 1180 K, and they have been analyzed and interpreted using several simple models. The distorted octahedral crystal field at the Zr site produced a (low-frequency) static electric quadrupole interaction which can be accurately described by the point-charge model. But, the temperature dependence of the associated electric field gradient (EFG) cannot be described accurately by purely static considerations via the point-charge model and high-temperature x-ray diffraction data. Although a high-frequency static interaction was also observed, the measurements were not sufficiently accurate to identify its origin unambiguously. Some of the high-temperature measurements show evidence of a time-varying interaction, which may result from Ca^{2+}-ion jumping. But, jump frequencies derived classically from high-temperature electrical dc conductivity measurements are too low to agree with those indicated by the PAC data. However, the dc conductivity measurements support a simple model of thermally activated Ca^{2+}-ion transport. The temperature dependence of the EFG (corresponding to the low-frequency interaction) was used to determine an effective Debye-Waller factor. As a result of using this approach to analyze this type of PAC data, this factor was shown also to agree qualitatively with the predictions of the Debye crystal model, although significant theoretical limitations were encountered. These particular results suggest that the PAC technique may provide new insights into understanding advanced ceramic materials.

I. INTRODUCTION

Calcium zirconium phosphate (CZP), $CaZr_4P_6O_{24}$, is a member of a relatively new structural family of ceramics that have near-zero coefficients of thermal expansion,[1-7] and these ceramics are also the basis for superionic conductors.[6] (Hazen *et al.*[3] describe the structure of the best-known superionic conductor, "nasicon," and we use their structural data in lieu of high-temperature x-ray data for CZP.) Because this family has been examined by high-temperature x-ray diffraction[3] and because CZP is thermally stable over a large range of temperature, CZP is, therefore, a good candidate for investigation by a nanometer-scale technique such as perturbed angular correlation (PAC) spectroscopy. Moreover, although these materials are important to several technologies (for example, high-temperature battery technology), no techniques such as PAC have been applied to obtaining a fundamental understanding of the structural properties of these materials.

The PAC technique uses radioactive probe atoms that have rather special nuclear properties to measure electric field gradients (EFG's), magnetic hyperfine fields, and spin-relaxation mechanisms at the sites of the probe atoms. Generally, in solid-state systems these probe atoms substitute in small or trace amounts for a specific type of atom in the lattice. For example, to study CZP, Hf atoms were substituted into the Zr sites in CZP. In this study we have addressed several major issues which are the following.

(1) Since the Zr sites in CZP have distorted octahedral nearest-neighbor environments, does the $^{181}Hf/^{181}Ta$ probe undergo a static electric quadrupole interaction at the Zr site?

(2) If so, can the interaction be accurately described by a simple model, e.g., the point-charge model?

(3) At what temperatures do nuclear-spin-relaxation effects appear?

(4) Can the temperature dependence of the EFG associated with the static interaction be described theoretically?

Before presenting the details of the investigation, we discuss these issues in more detail.

Figure 1 shows the crystal structure of CZP. X-ray diffraction structure determinations of CZP (Ref. 5) as

well as those of closely related materials[3] show that the six-coordinate Zr-nearest-neighbor O-atom environment has a distorted octahedral structure. For this reason we expect a static interaction of the ^{181}Ta (produced by β^- decay of ^{181}Hf) quadrupole moments with the EFG's produced primarily by the electrons of the Ta atoms and those of the nearest-neighbor O atoms. The point-charge model has been used effectively by others in relating PAC-determined EFG's to structure,[8] although more sophisticated models exist and have been used such as the angular-overlap model.[9] In the case of CZP, we expect the model to work well because the crystal is ionic. More importantly, the model allows comparisons to be made between structural changes discerned from x-ray diffraction measurements made at elevated temperatures and the structural changes inferred from the measured EFG's.

In addition, the PAC technique may yield information about defects in CZP, because the technique has been used to characterize defects in metals[10,11] and in semiconductors.[12] Also, the technique may provide information about cation transport. Rapid transport of Ca^{2+} ions which occurs in CZP at high temperatures may give rise to nuclear spin relaxation in which the resulting attenuation of the angular correlation may reflect the rate of Ca^{2+} ions "jumping" from site to site.

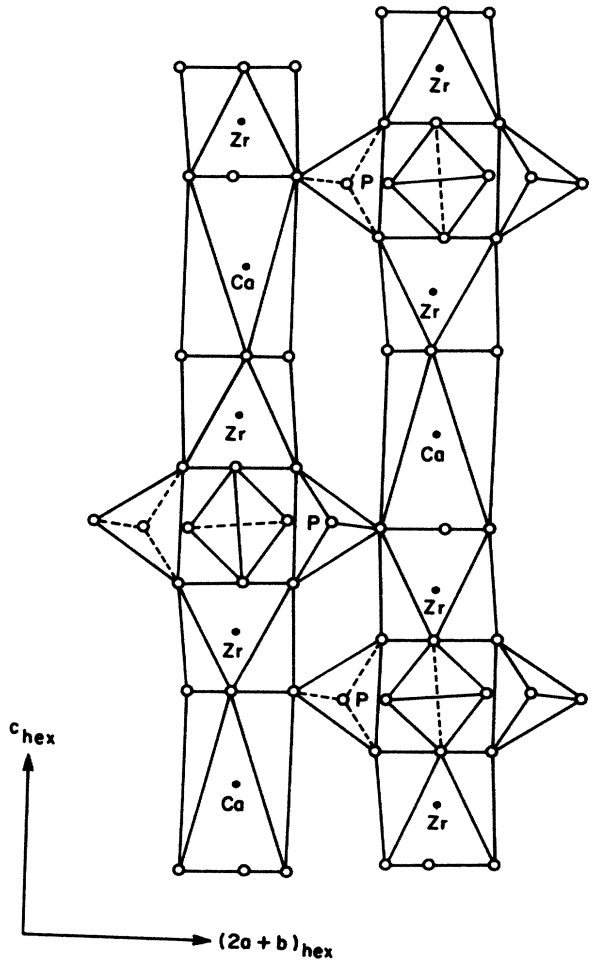

FIG. 1. The basic structure of CZP. For more details see Refs. 1 and 3. Note that only half of the labeled Ca sites can be occupied in the actual structure.

Currently, there is no theoretical basis for quantitatively predicting the temperature dependence of the EFG at the Zr site which arises from the distortion of the octahedral, nearest-neighbor configuration of O atoms. This problem is common to PAC studies of many insulators and semiconductors. Also, this situation is in contradistinction to the theoretical understanding of the EFG temperature dependence in metals. Dating back to the early 1950's, much theoretical and experimental work has been done in the case of metals, which has been reviewed.[13,14] Empirically EFG's in both cubic and noncubic metals exhibit a $\frac{3}{2}$ power-law decrease with temperature. During the last 15 years, additional theoretical work has contributed more understanding to this phenomenon.[15–21]

In fact, the literature is particularly confusing and contradictory on the subject of the temperature dependence of the EFG in semiconductors and in insulators. For example, measurements on InSe, a semiconductor, show a $T^{3/2}$ power-law decrease of the EFG with temperature, whereas those on InS and InTe show increases in the respective EFG's with temperature. Also, In_2Se_3 and In_2Te_3 show temperature dependences that are different than those shown by InSe or InS.[22] Other similar studies show different dependences of the EFG on temperature which may result from differences in stoichiometry and phase,[23–25] modulation of the static EFG,[26] electrical history,[27] and other factors.[28] In the case of insulators, the situation also lacks both a theoretical and an experimental codification. For example, Barfusz *et al.*[29] report that hafnium oxide exhibits no temperature dependence of the EFG over a range from 77 to 1500 K, which they attribute to the large band gap in this insulator. This conclusion is surprising because lattice dynamics, i.e., vibrational degrees of freedom, appear to be responsible for the effect in metals. Although Jaeger *et al.*[30] observe a slightly decreasing dependence for monoclinic zirconium oxide, their data on yttrium-oxide-stabilized zirconium oxide show a marked decrease in the EFG with temperature. Thus, the band-gap consideration in this case is somewhat of a canard. In a study of another insulator, K_2HfF_6, Caracoche *et al.*[31] focus primarily on time-varying interactions occurring at elevated temperatures. Although they have observed an EFG for a static interaction that slowly decreases with temperature, they do not offer any comment. A study by Martínez *et al.*[32] on a similar fluoride, $(NH_3)_2HfF_6$, has revealed that the EFG temperature dependences of the two inequivalent Hf sites are different; the EFG for one site increases with temperature, the other decreases. Additionally, studies on other similar fluoride insulators show some dissimilar features.[33–35] Because these experiments show little commonality in the temperature dependence of the EFG in insulators and because little theoretical guidance on this subject is available for complex, polycrystalline insulators, we have attempted to apply some of the theory that has been used to analyze the temperature dependence of the EFG in metals. And, in the case of CZP, in

which the temperature dependence of the EFG cannot be explained by purely static structural considerations, the analysis has produced an effective Debye-Waller factor which is discussed in detail below.

II. EXPERIMENTAL DETAILS

A. Sample Preparation

The $CaZr_{3.95}Hf_{0.05}P_6O_{24}$ samples were synthesized by the well-known sol-gel technique, which is used for the preparation of a wide variety of ceramic materials. This technique uses aqueous solutions of soluble inorganic salts or metal alkoxides as precursors. In this preparation, the starting materials were the aqueous solutions of $Ca(NO_3)_2 \cdot 4H_2O$, $HfOCl_2 \cdot 8H_2O$, $ZrOCl_2 \cdot H_2O$, and $NH_4H_2PO_4$. Stoichiometric amounts of these solutions were mixed to form a gel. The sequence of mixing of individual components was critical to forming a gel of uniform composition and to obtaining a single-phase material. The starting precursor solution was calcium nitrate to which zirconyl chloride was added followed by hafnyl chloride. Finally, the aqueous solution of ammonium dihydrogen phosphate was added drop by drop to the main solution while the solution was constantly stirred. All mixings were carried out at laboratory temperature. Progressive addition of the phosphate solution led to gradually increasing viscosity as the gel formed. This gel was dried at 353 K for about 20 hours to form a weakly cross-linked mass. Then, the material was hand crushed with a mortar and pestle to a powder form which was calcined at 970 K for 16 hours to drive off the volatile species such as NO_2, NH_3, Cl_2, and H_2O. The partially reacted calcined material was grounded to a -325 mesh powder and a polyvinyl alcohol binder was added. This powder was pressed into rectangular bars and then sintered at 1570 K for 24 hours. After sintering, samples were cut having masses of approximately 0.5 g. After the sample preparation was completed, an x-ray diffraction powder pattern was measured to make sure that Hf substituted for Zr in the structure, and no evidence of a second phase, e.g., HfO_2, was found.

These samples were irradiated in the Pennsylvania State University Breazeale Reactor to produce the ^{181}Hf activity. Because an initial PAC measurement on an unannealed sample showed evidence of inhomogeneous line broadening, the samples were annealed at 1270 K for approximately 36 hours. As a result of this annealing, the anisotropy of the data taken subsequently increased. Also sufficient time was allowed to pass so that the ^{95}Nb interference (produced by Zr activation) decayed to an insignificant level.

B. PAC measurements

1. Technical details

The PAC measurements used $^{181}Hf/^{181}Ta$ as the probe for which Fig. 2 gives the decay scheme and the relevant nuclear data. The PAC apparatus was a four-detector system which Fig. 3 shows schematically. The detectors

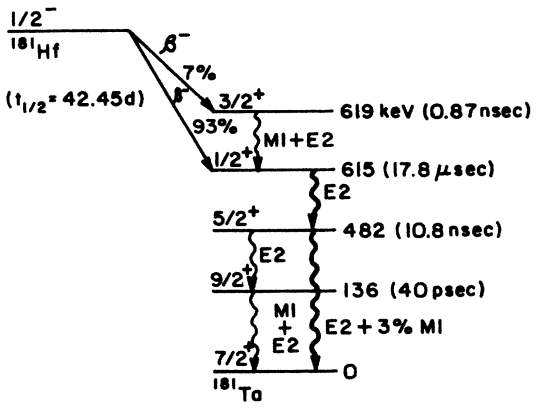

FIG. 2. A simplified decay scheme for the PAC probe $^{181}Hf/^{181}Ta$. The quadrupole moment of 2.51*b* was taken from G. Netz and E. Bodenstedt, Nucl. Phys. A **208**, 503 (1973). The other data were taken from *Table of Isotopes*, 7th ed., edited by C. M. Lederer and V. S. Shirley (Wiley, New York, 1978), pp. 1133–1135. Notice that a state having a half-life of 17.8 μsec precedes the γ-γ cascade of interest, i.e., 133–482 keV; this long-lived state assures that the effects of nuclear recoil and electronic rearrangement have equilibrated before the cascade occurs.

were CsF scintillation crystals which provided a nominal time resolution of 0.9 ± 0.1 full width at half maximum nsec (FWHM) (5.08×5.08 cm^2 for the 482-keV photons and 5.08×1.27 cm^2 for the 133-keV photons). Source-to-detector distances were nominally 15 cm, and W and Cu foils were usually used to absorb low-energy γ rays and x rays, respectively. Typically, Hamamatsu R329 and R1332 photomultiplier tubes were used. Start and stop signals were provided by ORTEC model No. 583 constant-fraction differential discriminators, which also were operated to give coarse energy discrimination. The slow-coincidence electronics provided finer energy discrimination. Four coincidences, in this case two 90°-90° and two 180°-180°, were measured independently via individual time-to-amplitude converters (TAC), which were conversion-gain matched using an ORTEC model No. 462 time calibrator. Signals from each TAC were routed via a multiplexer to the respective 1024-channel segment of the pulse-height analyzer memory. A DEC PRO 350 microcomputer was used to store the data and to reformat the data for subsequent analysis. Source strengths were typically 50–80 μCi of ^{181}Hf. A ^{22}Na source was used to locate the time-zero channels and to measure the time resolution. A heater consisting of a fused-silica tube wrapped with nickel-chromium wire and insulation was used to make the elevated temperature measurements. Low-temperature measurements were made using a simple Dewar flask.

2. A summary of PAC theory

The theory of perturbed angular correlation gives the (arbitrarily normalized) correlation function $W(\theta,t)$ as

$$W(\theta,t)=\exp(-t/\tau_n)[1+A_{22}G_{22}(t)P_2(\cos\theta) + A_{44}G_{44}(t)P_4(\cos\theta)+\cdots], \quad (1)$$

in which t represents the time between the detection of the first γ ray and the detection of the second γ ray.[36] τ_n is the lifetime of the intermediate quantum state. The coefficients A_{22} and A_{44} contain the spatial correlation information and are time independent. The functions $G_{22}(t)$ and $G_{44}(t)$ are functions of time that describe the perturbation. For a polycrystalline solid, the perturbation function describing a static interaction is given by the Abragam and Pound expression[37]

$$G_{22}(t)=S_0+\sum_{k=1}^{3} S_k\cos(\omega_k t) . \quad (2)$$

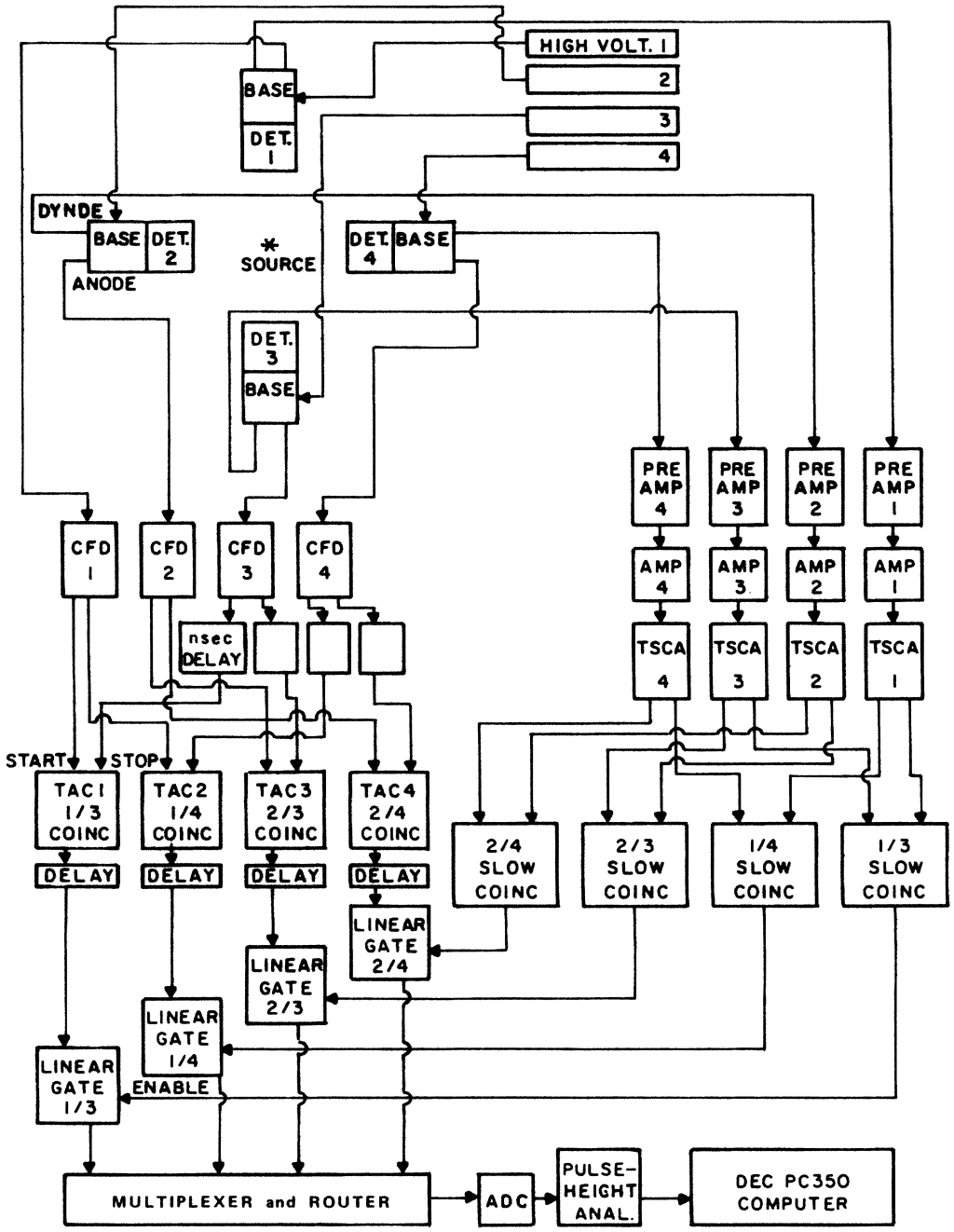

FIG. 3. The PAC experimental apparatus is shown schematically. The abbreviations are ADC (analog-to-digital converter); AMP (amplifier); CFD (constant-fraction-differential discriminator); PREAMP (preamplifier); TAC (time-to-amplitude converter); TSCA (timing single-channel analyzer).

The quadrupole frequency ω_Q is related to the zz component of the EFG, V_{zz}, in the principal-axis system by

$$\omega_Q = [eQV_{zz}/4I(2I-1)\hbar] , \tag{3}$$

in which Q is the nuclear quadrupole moment and I is the nuclear spin.[37] The frequencies ω_k in Eq. (2) are related to the quadrupole frequency ω_Q by Gerdau's method.[38] When the EFG has axial symmetry, i.e., equivalence of the x and y directions, $\omega_Q = \omega_1/6$, $\omega_2 = 2\omega_1$, and $\omega_3 = 3\omega_1$ (for $I = \frac{5}{2}$). The deviation from axial symmetry is given by the asymmetry parameter η,

$$\eta = (V_{xx} - V_{yy})/V_{zz} . \tag{4}$$

The experimentally derived parameters ω_Q and η completely describe the EFG tensor in the principal-axis system because

$$V_{xx} + V_{yy} + V_{zz} = 0 \tag{5}$$

and

$$\omega_3 = \omega_1 + \omega_2 . \tag{6}$$

Interactions with time-varying EFG's can be described in terms of a rotational correlation time τ_c and an average quadrupole frequency $\bar{\omega}_Q$ for the limiting condition $\tau_c \ll 1/\bar{\omega}_Q$.

For this case, Abragam and Pound have derived[37]

$$G_{22}(t) = \exp(-\lambda_{22} t) , \tag{7}$$

in which

$$\lambda_{22} = \tfrac{18}{5}[4I(I+1) - 7]\bar{\omega}_Q^2 \tau_c . \tag{8}$$

When the limiting condition does not apply, other stochastic models may be used, which do not always yield closed-form expressions for $G_{22}(t)$.[39–41]

3. *Data analysis*

Four correlation functions $W_{jk}(\theta_{jk}, t_i)$ represent the primary experimental data (the subscripts j and k refer to the coincidence between the respective detectors). The experimental perturbation function $A_{22}G_{22}(t_i)$ is obtained by forming the ratio

$$R(t_i) = \frac{2}{3}\left[\left[\frac{W'_{13}(180°, t_i)W'_{24}(180°, t_i)}{W'_{14}(90°, t_i)W'_{23}(90°, t_i)}\right]^{1/2} - 1\right] , \tag{9}$$

in which the primes indicate that corrections for random coincidences have been made. This ratio (when $A_{44} = 0$) is related to the perturbation function by

$$A_{22}G_{22}(t_i) = R(t_i)/\{1 + [R(t_i)/2]\} . \tag{10}$$

To obtain the PAC parameters from the experimental perturbation functions, a two-site model based on Eq. (2) was used to fit the data:

$$A_{22}G_{22}(t_i) = A_1\left[S_0 + \sum_{k=1}^{3} S_k \exp(-\tfrac{1}{2}\omega_k \delta_1 t_i)\cos(\omega_k t_i)\right] + A_2\left[S_0 + \sum_{k=4}^{6} S_k \exp(-\tfrac{1}{2}\omega_k \delta_2 t_i) \times \cos(\omega_k t_i)\right] + A_3 . \tag{11}$$

A_1 and A_2 are the normalization factors, A_3 is a "background" term, δ_1 and δ_2 are the parameters that take into account line broadening via a Lorenzian line shape. When the experimental data showed evidence of a time-varying interaction, the fitting function was modified by multiplying A_1 and A_2 in Eq. (11) by $\exp(-\lambda_{22} t_i)$ in which λ_{22} is a "damping" parameter. For simplicity, since $A_1 \gg A_2$ in this case, only one damping factor was used, although a separate factor could have been used for each site. The fitting algorithm, which was implemented by a FORTRAN computer program, was based on the Gauss-Newton nonlinear regression method, which was modified to weigh the squared errors by the inverse squares of the experimental uncertainties,[42] and the constraints, $\omega_1 + \omega_2 = \omega_3$ and $\omega_4 + \omega_5 = \omega_6$ were applied. Generally, the initial values of the frequencies were obtained from Fourier transforms of the data. Error estimates for the frequencies were obtained from the regression analysis. Additionally, data points for the first few time intervals were not used in the analysis because they contained information from the prompt 346-keV–136-keV cascade in ^{181}Ta, as a result of the limited energy resolution of the CsF scintillation detectors.

C. Conductivity measurements

To determine the extent of Ca^{2+}-ion motion at high temperatures, dc conductivity measurements were performed. A CZP specimen was diamond sawed to a planar rectangular shape $\sim 1 \times 1 \times 0.5$ cm.^{3} Ion-blocking, nonfritted platinum electrodes were applied to parallel sides and fired on at 1070 K for two hours. The two-probe, low-field (20 V/cm) dc conductivity was measured from 298 to 1270 K using a Keithley Model No. 610 picoameter (sensitive to ~ 1 pA) and a Model No. 248 voltage supply, in conjunction with an alumina muffle tube furnance.[43] Platinum leads were in contact with the specimen, and they were connected via coaxial cable to the measurement system. The temperature was monitored to ± 1 K using a type-K thermocouple. The conductivity was measured during the heating of the sample and also during the cooling of the sample to check for possible electrode polarization caused by macroscopic Ca^{2+}-ion motion.

III. RESULTS

A. The primary data

Figure 4 presents the experimental perturbation functions and the fitted theoretical functions. In addition to performing free-parameter fits to Eq. (11), we checked the

effect of the constraint, $\eta=0$. For the purposes of comparison, both fits are given with the data for 291 K, and the free-parameter fit is qualitatively better. With the exception of the perturbation functions for 966 and 1180 K, no damping factors were used. To fit the 966-K and the 1180-K data sets, the damping factor was used, but, in both cases, the fits are poor at large times. All of the parameters derived from the 1180-K data are uncertain and cannot be considered unique. For example, several fits to the data for 1180 K produced damping factors that varied by factors of 2–3 from fit to fit, and the associated variations in the δ and A parameters were also observed. Thus, unique parameter set could not be obtained for the 1180-K data. Also, two runs were done at 291 K, one before the high-temperature series of runs and one after, and the derived parameters ω_Q and η agree. This result indicates that the CZP structure does not exhibit a temperature "memory" effect.

Figure 5 presents the derived quadrupole frequencies ω_Q for the low-frequency and the high-frequency interactions. Figure 6 presents the other parameters. In general, the parameters describing the high-frequency interaction show much larger uncertainties than the low-frequency-interaction parameters. This feature is a consequence of the fitting procedure being insensitive to small site populations. The populations $[A_i/(A_1+A_2+A_3)]$ are approximately 80% for the sites experiencing the low-frequency interaction and 10–20% for other sites. Hence, obtaining accurate detailed information about the high-frequency interaction is problematical. The asymmetry parameters η are relatively small for the low-frequency interaction. This result is consistent with the axially symmetric nearest-neighbor environment of the Zr site, which is known from the x-ray diffraction structural information. Interestingly, with few exceptions, the linewidth parameters δ remain relatively small over most of the temperature range. Also, with the exception of the data obtained at 77 K, the anisotropy appears to be approximately one-half of that expected from an unperturbed correlation [$A_{22}\cong 0.23$,

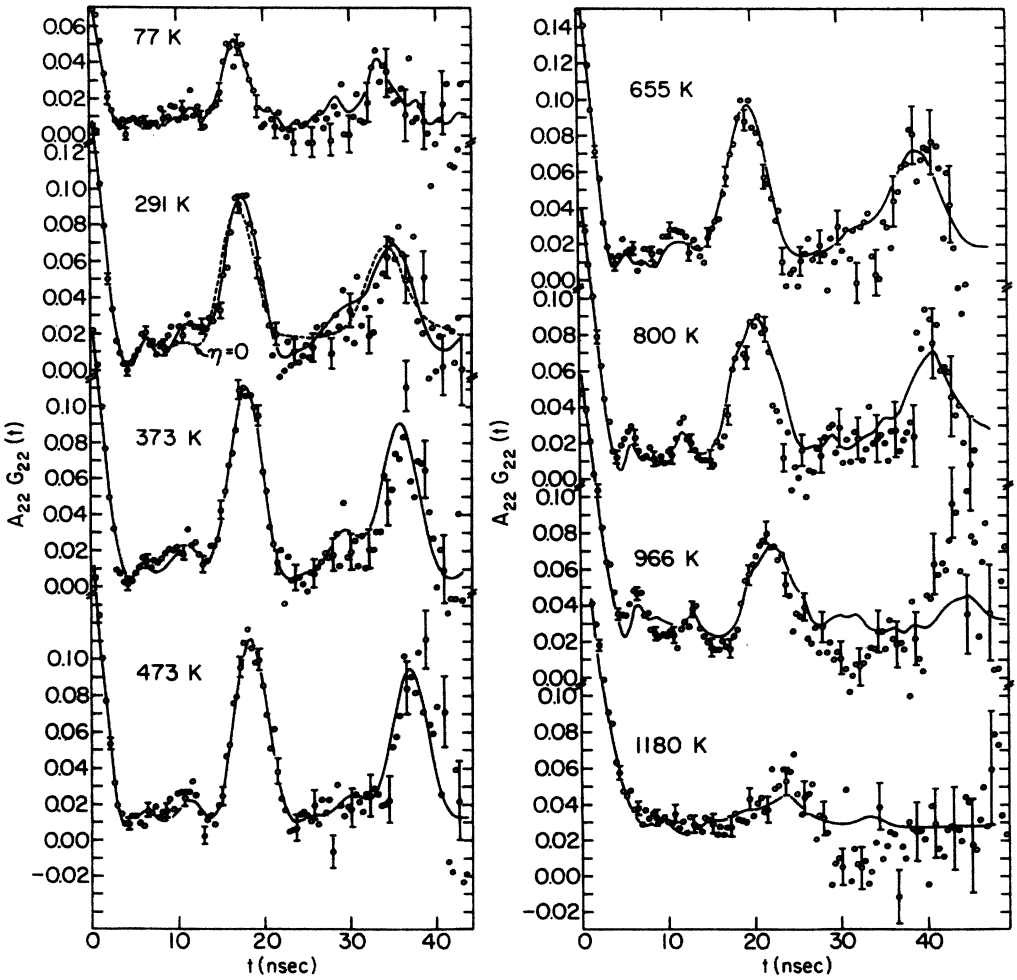

FIG. 4. Perturbation functions for $CaZr_{3.95}Hf_{0.05}P_6O_{24}$ for measurements performed at the indicated temperatures. The solid lines represent fits to the two-site model. For the 291-K data, the curve labeled $\eta=0$ represents a fit constrained with $\omega_2=2\omega_1$ and $\omega_5=2\omega_4$.

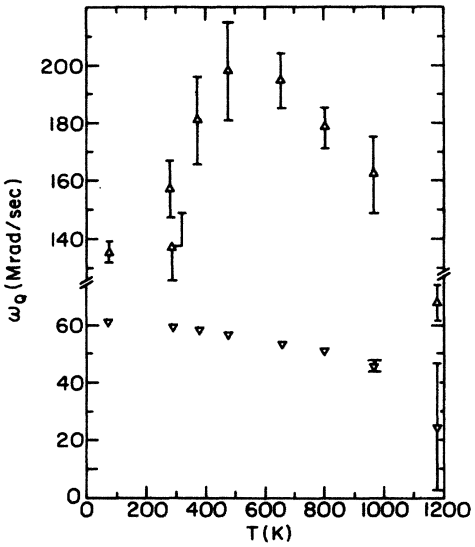

FIG. 5. The derived quadrupole frequencies are shown for the two sites. For the low-frequency points, unless otherwise shown, the uncertainties are no greater than the size of the data points.

which we determined from a measurement on HfF_6^{2-} (Ref. 44)]. The perturbation function for 77 K shows approximately one-half of the anisotropy of the other perturbation functions. This effect results from γ rays scattering in the Dewar flask or in the liquid nitrogen, as we have observed the effect in other PAC experiments.

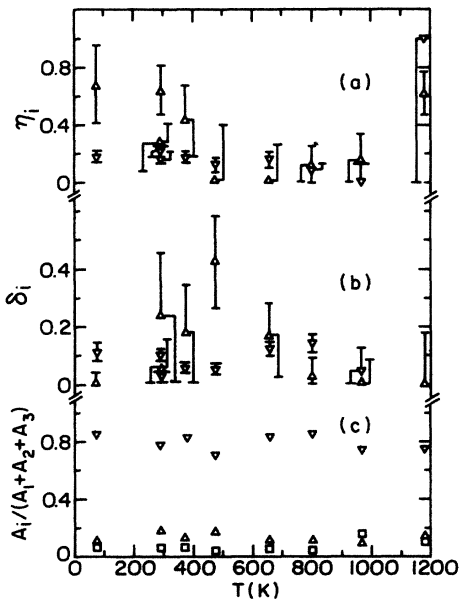

FIG. 6. (a) The asymmetry parameters for both sites are presented. The inverted triangles refer to site 1, which experiences the low-frequency interaction, and the triangles to site 2, which experiences the high-frequency interaction. (b) The linewidth parameters δ_1 and δ_2 are shown. (c) The site populations are shown. The ratio $(A_i/(A_1+A_2+A_3)$ refers to Eq. (11); the squares refer to A_3.

To summarize the overall picture of the primary PAC data, we mention that the major interaction occurs at low frequencies with small asymmetry parameters, and the frequencies decrease with temperature while the asymmetry parameters remain relatively constant. Finally, the character of the perturbation function appears to be different at 966 K and 1180 K. At 966 K, a time-varying interaction appears along with the static low-frequency and high-frequency interactions. And at 1180 K, the static interactions are no longer well defined. Unfortunately, there are no other experimental data available to confirm whether a phase change occurs between 966 and 1180 K.

B. Conductivity measurements

Figure 7 presents the dc conductivity data which follow an Arrhenius relationship:

$$\sigma(T)=\sigma_0\exp(-\Phi/k_BT)\ , \tag{12}$$

in which σ is the conductivity in $\text{ohm}^{-1}\text{cm}^{-1}$, σ_0 is the pre-exponential factor, Φ is the activation energy, k_B is the Boltzmann constant, and T is the absolute temperature. In this case the derived activation energy is 1.4 eV. For ionic conductors in which the carrier concentration is fixed, as is the case for CZP, the activation energy is strictly associated with the ionic mobility. High-

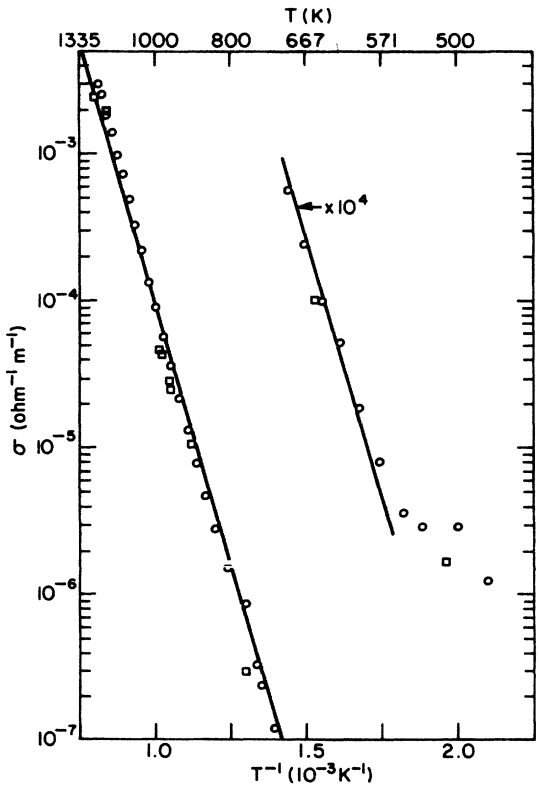

FIG. 7. The conductivity of a sample of the CZP ceramic is shown as a function of inverse temperature. The circles refer to measurements during the cool-down phase, the squares, to the heat-up phase.

temperature conductivity values range from 5×10^{-7} ohm^{-1}cm^{-1} at 966 K to 1×10^{-5} ohm^{-1}cm^{-1} at 1180 K. Additionally, the absence of an inflection in the high-temperature portion of the data in Fig. 7 indicates that electronic conduction is not significant at these temperatures. For interstitial diffusion of Ca^{2+} ions, the Nernst-Einstein equation relates the diffusion coefficient D_r to the conductivity,

$$\sigma(T)=(cZ^2e^2/k_BT)D_r \ , \tag{13}$$

in which Z is the valence and c is the concentration of the Ca^{2+} ions. The diffusion coefficient is related to the jump frequency of the Ca^{2+} ions, ω, by

$$D_r=\omega s^2/6 \ , \tag{14}$$

in which s is the interstitial jump distance. Given Eqs. (12), (13), and (14) and the experimentally determined activation energy of 1.4 eV, we can make a one-to-one correspondence between the conductivity values at each temperature and the jump frequency. Taking 3.3 Å (the normal Ca-to-Zr distance) as an estimate of the jump distance, we find that the jump frequency varies from $\sim2\times10^5$ jumps/sec at 966 K to $\sim5\times10^6$ jumps/sec at 1180 K. Although dc conductivity measurements are limited to their information content relative to ac measurements, these dc measurements are adequate for testing a very simple model, i.e., Eqs. (12), (13), and (14).

IV. INTERPRETATION AND DISCUSSION

A. The point-charge model

To determine how purely static considerations affect the temperature dependence of the EFG, we consider the low-frequency interaction by examining the structure of the nearest-neighbor configuration of the Zr site. An extensive amount of x-ray diffraction data has been obtained over a range of temperatures from 298 to 963 K on an isomorphic material, $Na_{1.11}Zr_2P_{2.89}Si_{0.11}O_{12}$.[3] We have used the structural data for this Na analog to obtain Cartesian coordinates for the distorted octahedron which is formed by the six O atoms in the vicinity of the Zr site. Although the CZP lattice differs from that of the Na analog in several minor aspects, the most consistent approach—given the lack of direct CZP data—is to use the Na analog data to approximate the Zr octahedra in the CZP structure. It is convenient to choose the C_3 axis as the z axis for the distorted octahedron because the C_3 axis, also a principal axis, is parallel to the c axis of the unit cell.

The usual representation of the EFG, $eq=V_{zz}$, in the principal-axis system is given by[14]

$$eq=(1-\gamma_\infty)eq_{\rm ion}+(1-R)eq_{\rm el} \ , \tag{15}$$

in which $(1-\gamma_\infty)$ and $(1-R)$ are the Sternheimer antishielding factors, $q_{\rm ion}$ refers to the EFG produced by all of the ions in the lattice except for the probe ion, and $q_{\rm el}$ refers to the EFG produced by conduction electrons.[14] The antishielding factor $(1-\gamma_\infty)$, which represents primarily the polarization of the probe ion electron cloud by the nuclear quadrupole moment,[14,45] is taken as 62 from Feiock and Johnson.[46] The $(1-R)$ factor is not well known, and R is often taken as zero;[14,15] similarly, $q_{\rm el}$ is thought to be insignificant in this case. Also, we approximate the effects of all of the ions in the lattice by the nearest-neighbor configuration.

Now, the point-charge model for the nearest-neighbor configuration of N ions is given by

$$eq=e(1-\gamma_\infty)\sum_{i=1}^{N} Z_i(3z_i^2-r_i^2)/r_i^5 \ , \tag{16}$$

in which Z_i is the charge on the ith ion.[47] In these calculations we take the O-ion charge as the formal charge, namely, -2. We consider the case of the distorted octahedral configurations of six O ions at four temperatures. The distorted octahedral system of ions should be in the principal-axis system, and we confirmed this assumption by calculating the entire tensor and checking that the off-diagonal elements vanish.[47]

The point-charge model does account for the low-frequency interaction. The model gives a calculated value of -7.0×10^{17} V/cm^2, which has a magnitude approximately 15% greater than the measured value of $6.16\pm0.07\times10^{17}$ V/cm^2. Figure 8 shows the resulting values, which have been normalized to the low-temperature (291 K) experimental values, along with the values of V_{zz} derived from the ω_Q values. The effect of increasing the temperature is to decrease the magnitude of the EFG. But, notice that the decrease shown by the calculated values is much less than the decrease shown by the experimental values. This last result indicates that a purely static description of the EFG is not sufficient to describe its temperature dependence.

We also attempted to account for the high-frequency interaction by considering the effects of the EFG of (1) an O vacancy and (2) a Ca^{2+} ion in several interstitial posi-

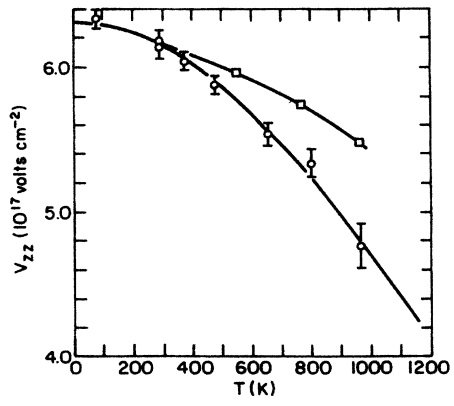

FIG. 8. The temperature dependence of the zz component of the EFG is shown for the low-frequency interaction. The solid line represents a linear least-squares fit to a Gaussian function. The error bars reflect uncertainties in the values of ω_Q from which these values were derived. The normalized results of the point-charge model (squares) are also shown where the line has been drawn to guide the eye.

tions. Unfortunately, because the high-frequency data have large uncertainties and because these two possibilities are only two out of many, we were unable to make a unique accounting.

B. Conductivity measurements

For CZP, the activation energy of conduction is associated strictly with the Ca^{2+} mobility, which depends primarily on three factors: (1) the size of the opening through which the Ca^{2+} ions move, (2) the ionic bond strengths of the Ca^{2+} ions at the initial site and at the final site, and (3) a factor related to the strength of the oxygen-ion bonds forming the opening. In essence, the activation energy reflects the strain energy necessary to displace neighboring atoms so that the mobile ion can jump from the initial site to the final site.

In order to understand the significance of the magnitude of the measured conductivity and the associated activation energy, we examine an isomorphic material, $Na_{4-x}Zr_xSi_{3-x}P_xO_{12}$ (NZP).[6,48–57] The technological importance of NZP, which lies in liquid sodium battery applications, arises from its high, "superionic" conductivity (10^{-4} ohm^{-1}cm^{-1} at 298 K). This high ionic conductivity is produced by the three-dimensional mobility of the Na^+ ions in the structure. The low activation energy, 0.28 eV, reflects the low strain energy produced by the Na^+ ions in the bonds of the other atoms along the preferred conduction pathways in the structure. At laboratory temperature, the measured conductivity of NZP is $\sim$6–7 orders of magnitude greater than that of CZP (which is reflected by the large activation energy of 1.4 eV), and the ionic radii of the Ca^{2+} and Na^+ ions are 0.99 and 0.94 Å, respectively. Therefore, the associated differences in the conductivities and in the activation energies do not result from the effects of strain energy produced during diffusion. But, rather, these differences result primarily from the ionic charge differences. That is, the higher charge of the Ca^{2+} ion increases the ionic bond strength for this ion at the Ca sites in the lattice. As a result, the Ca^{2+} ions do not jump very frequently at low temperatures.

As mentioned above, the jump frequency for Ca^{2+} ions is approximately 2×10^5 jumps/sec at 966 K and 5×10^6 jumps/sec at 1180 K. In terms of spin-relaxation effects, Baudry *et al.*[58] who considered the effects of oxygen-vacancy transport in oxygen-defective zirconias and who cited the results obtained from a stochastic model developed by Winkler and Gerdau,[39] mention that values $<10^8$ sec^{-1} fall into the low jump-frequency limit, in which $\lambda_{22}=\omega$, the jump frequency. In the damping factor, $\exp(-\lambda_{22}t)$, used with Eq. (11) for the data taken at 966 K, the parameter λ_{22} was found to be 4×10^7 sec^{-1}, and this result is significantly larger than the jump frequency derived from the conductivity data. This lack of agreement may simply be the consequence of several factors such as the crudeness of the model, i.e., Eqs. (12), (13), and (14), or a systematic error in the magnitudes of the measured conductivities,[43] or the limitations of the dc technique. Alternatively, Ca^{2+}-ion motion may be more efficient in relaxing spins than in carrying current. Currently, ac measurements are being made to address these issues. Nonetheless, the high-temperature perturbation functions appear to be showing the effect of relatively infrequent but relatively strong instantaneous changes in the EFG, which occur during the γ-γ cascade in ^{181}Ta.

C. The temperature dependence of the EFG

In this section we focus on the dependence of the low-frequency interaction on temperature. Before considering the effects of lattice vibrations on the EFG, we briefly mention more about the results of the elevated-temperature x-ray diffraction measurements.

To understand the results that follow, we have to visualize the distorted octahedral structure along the z-(C_3) axis as a projection of the O-ion positions into the x-y plane. Here, the six ions form two overlapping equilateral triangles. In an undistorted octahedron, the six vertices would be equally spaced at 60°. But, in this structure, the vertices of one of the triangles is displaced several degrees with respect to the vertices of the other, and the z coordinates of the two triangles are not equal in magnitude, i.e., the Zr site is not at the center of the octahedron. As the temperature increases, the orientation of the one triangle changes with respect to the other by several degrees.[3] A sizable effect arises because the CZP structure undergoes an increase in the c parameter and a corresponding decrease in the a parameter as temperature increases.[1] Overall, as the temperature increases, the octahedral configuration becomes more symmetric, i.e., less distorted, and the corresponding values of V_{zz} decrease in magnitude. But, the effect is not nearly large enough to account for the experimental result.

Now, we focus on the temperature dependence of the EFG, which is shown in Fig. 8, in the context of lattice dynamics. The curve in Fig. 8 is a fit to a Gaussian function:

$$V_{zz}(T)=V_{zz}(0)\exp(-bT^2)\ . \tag{17}$$

This function fits the data quite well, and it is interesting and clear that the temperature dependence is neither linear nor $T^{3/2}$. To obtain a theoretical basis for the apparently good representation of the data by this function, we consider the result derived by Nishiyama *et al.*,[17,20]

$$eq(T)=(1-\gamma_{\rm eff})eq^{\rm sc}_{\rm ion}(T)\exp[-\tfrac{4}{3}k_F^2\langle u^2\rangle(T)]\ . \tag{18}$$

This result is based on the *ansatz* represented by Eq. (16). The factor $(1-\gamma_{\rm eff})$ is an antishielding factor which is taken to be temperature independent, $eq^{\rm sc}_{\rm ion}$ is a lattice sum calculated using a pseudopotential method, k_F is the wave-vector magnitude at the Fermi energy, and $\langle u^2\rangle$ is the mean-square vibrational amplitude for an atom in the lattice. The exponential factor is known as the Debye-Waller factor (DWF). This expression was applied specifically to monatomic metal lattices. They have calculated $eq^{\rm sc}_{\rm ion}$ and have obtained the DWF's from experimental data, and their work has produced the $(1-\alpha T^{3/2})$ functional dependence of eq on temperature, which in metals has been almost universally observed.[59] Our ap-

proach is to make a correspondence between Eq. (18) and Eq. (17). In Eq. (18), $eq(T)$ is given as the product of an antishielding factor, a factor that depends on the equilibrium positions of the atoms (ions) in the lattice, namely, $eq_{\text{ion}}^{\text{sc}}$, and a DWF, which is strongly temperature dependent. Equation (17) gives $V_{zz}(T)$ as the product of a factor that depends primarily on the equilibrium positions of the atoms at a temperature of zero degrees, namely, $V_{zz}(0)$, and the factor, $\exp(-bT^2)$, which in this correspondence is an effective DWF. In the approach of Nishiyama *et al.*[17,20] the Fermi wave-vector magnitude k_F refers to a gas of conduction electrons in a metal. Also, in their DWF, they introduce a factor of $\frac{1}{3}$ which refers to a threefold degeneracy of the wave vectors.

Given this correspondence, we can develop an expression for a DWF specifically for CZP or other similar ionic crystals. The objective is to see whether we can develop a physically reasonable expression for the value of the b parameter in Eq. (17). Because we are dealing with an insulator, CZP, we replace k_F with the Debye wave vector k_D and $k_D=(6\pi^2 n_{\text{ion}})^{1/3}$ in which n_{ion} is the number of ions per unit volume of crystal (this definition is purposely vague). Also, we drop the factor of $\frac{1}{3}$, although this action is not critical. The DWF is usually denoted by $\exp(-2W)$; hence we have

$$-2W=-4k_D^2\langle u^2\rangle \ . \tag{19}$$

To obtain the mean-square displacement $\langle u^2\rangle$, we use the Debye model of a crystal. Using the standard expressions, the mean-square displacement has been derived for a monoatomic crystal:[60]

$$\langle u^2\rangle=\frac{3\hbar^2T^2}{Mk_B\Theta_D^3}\left[\frac{\Theta_D^2}{4T^2}+\int_0^{\Theta_D/T}\frac{x\,dx}{(e^x-1)}\right], \tag{20}$$

in which M is the mass of the atom, k_B is the Boltzmann constant, and Θ_D is the Debye temperature. We obtain for the DWF:

$$\exp(-2W)=\exp\left[\frac{-12k_D^2\hbar^2T^2}{Mk_B\Theta_D^3}\times\left[\frac{\Theta_D^2}{4T^2}+\int_0^{\Theta_D/T}\frac{x\,dx}{(e^x-1)}\right]\right]. \tag{21}$$

This expression for the DWF applies rigorously to a monatomic crystal (having atoms of mass M) that is harmonic and that obeys the Debye dispersion relation $\omega=ck$. Unfortunately, CZP is not monatomic and, more importantly, CZP is not harmonic. A nonzero coefficient of thermal expression indicates that the crystal is anharmonic. But, the case of CZP is peculiar, because its coefficient of thermal expansion has a *very small* magnitude but the a and c parameters change significantly with temperature.[1] Thus, CZP is an anharmonic crystal. Furthermore, an analysis of specific-heat data[61] on a closely related material, $Ca_{0.9}Sr_{0.1}Zr_4P_6O_{24}$, yields no distinct Debye temperature. (For specific heats measured at four temperatures between 300 and 470 K, the Debye temperatures range from approximately 2000 to 1250 K, respectively.) Thus, the Debye model and the associated DWF given by Eq. (21) appear much too simplistic to accurately describe the temperature dependence of the CZP EFG.

Given these caveats, we continue despite the limitations of the theory. Now, the experimental results, namely, the data shown in Fig. 8, show a clear Gaussian dependence of V_{zz} on temperature. Initially, we attempted to fit Eq. (21) to these data allowing Θ_D to be the only free parameter. But we obtained essentially a linear temperature dependence, and the deviations of the fitted function from the data were unacceptable at low temperatures. The effect arose because Θ_D tended to be in the range of the experimental values of T. Since we know that the Debye temperature should be well in excess of the range of temperatures over which V_{zz} was measured, we set the integral in Eq. (20) equal to the asymptotic value for $(\Theta_D/T)\to\infty$, namely, $\pi^2/6$. This action forces the argument of the exponential function in Eq. (21) to have a strictly T^2 dependence. The resulting expression is

$$-2W=-\frac{3\hbar^2k_D^2}{Mk_B\Theta_D}-\frac{2\pi^2\hbar^2k_D^2}{Mk_B\Theta_D^3}T^2 \ . \tag{22}$$

Since the CZP structure is complex, we do not have any simple descriptions for calculating k_D and M. Also, the PAC measurement tends to be more sensitive to the nearest neighbor environment of the Zr site than to the unit cell as a whole. To deal with this lack of information, we make several different assumptions about k_D and M. Then, we set the coefficient of T^2 in Eq. (22) equal to b in Eq. (17). This equality allows us to calculate Θ_D. [Note that the first term in Eq. (22) is much less than unity so the exponential function of this term is essentially unity.] Table I summarizes this series of assumptions and the resulting set of calculated Debye temperatures. We see that the derived values of Θ_D are in or close to the range of those values of Θ_D mentioned above. Thus, the analysis is self-consistent. Also, by making k_D arbitrarily large, larger values of Θ_D would result.

This analysis relates the vibrational motion of the atoms in the CZP lattice to the EFG's at the Zr site, which we have used ^{181}Hf/^{181}Ta to measure. Moreover, the effective DWF, namely, the exponential factor in Eq. (17), can be qualitatively explained in the context of the Debye model, although a lack of information persists. Furthermore, from the results of the point-charge model, it is clear that static considerations alone do not predict the temperature dependence of the EFG.

We mention briefly that the indicated *correspondence* between the temperature dependence of the EFG in CZP and the associated DWF has technological importance. For example, consider the study of yttria-stabilized-zirconia ceramics by Jaeger *et al.*[30] They observe differences in the EFG temperature dependence that result from differences in the composition, i.e., the fraction of yttria, and differences in crystal structure, i.e., the phase(s) present. The function of the "stabilization" process is to extend the range of temperatures over which the structure remains cubic. But no attempts have been made to understand the stabilization phenomenon in

TABLE I. Estimation of an effective Debye temperature for three assumed conditions.

Assumption	k_D (cm^{-1})	M (u)	$(\Theta_D)^a$ (K)
k_D refers to the entire unit cell.[b] M is the average mass per atom.	1.6×10^8	28	670
k_D refers to the Zr coordination sphere. M is the O-Ta reduced mass.[c]	2.2×10^8	15	1020
k_D refers to the entire cell. M is the O mass.	1.6×10^8	16	800

[a]The Debye temperature is obtained from $(-2\pi^2k_D^2\hbar^2T^2/Mk_B\Theta_D^3)=-bT^2$.
[b]The volume of the unit cell is 1516.06 $Å^3$ (see Ref. 4) and the cell contains 105 atoms.
[c]The volume of the coordination sphere is based on a bond length of 2.09 Å and the sphere contains seven ions.

terms of the changes in the phonon distributions with temperature. This study suggests that PAC can be used to investigate the effects of vibrational motion on the structural stability of some kinds of ceramics.

V. CONCLUSIONS

The low-frequency interaction at the Zr site in CZP results from a distorted octahedral crystal field, and this effect is accounted for with reasonable accuracy by the point-charge model. But the static, point-charge model (based on high-temperature x-ray diffraction data) does not provide an accurate picture of the temperature dependence of the EFG, because this effect results primarily from changes in the phonon distribution with temperature. Ca^{2+}-ion jump frequencies that are derived from the high-temperature dc conductivity measurements are much smaller than those associated with nuclear spin relaxation. This result indicates that the time-varying interactions at high-temperatures in CZP need more investigation. In this context, the potential value of ac measurements needs to be investigated. Also, if another member of the CZP family could be found, which exhibits time-varying interactions over a large temperature range, sufficient data could be obtained to test a spin-relaxation theory.

The temperature dependence of the EFG resulting from the low-frequency interaction represents an effective Debye-Waller factor. Application of the Debye crystal model with suitable simplifying assumptions qualitatively reflects the effects of vibrational motion. Although more theoretical work is needed to obtain quantitative information about lattice dynamics, these results suggest that the PAC technique can play an important role in developing advanced ceramics materials.

ACKNOWLEDGMENTS

We thank Professor Morton Kaplan of the Carnegie-Mellon University, who generously allowed us to learn the PAC technique in his laboratory. We also wish to thank him for much technical advice and encouragement and for specifically pointing out the significance of vibrational motion on the EFG temperature dependence. We gratefully acknowledge financial support from the College of Engineering, the Department of Nuclear Engineering, and the FERMI Industrial Consortium. We acknowledge Mr. Ronald Eaken, Mr. Kenneth Rudy, Mr. Douglas Vonada, and the staff of the Pennsylvania State Breazeale Reactor Facility for technical support. We thank Professor Anthony J. Baratta for sharing some ideas as well as some equipment with us. We thank Professor Rustum Roy for his encouragement and suggestions.

[1]R. Roy, D. K. Agrawal, J. Alamo, and R. A. Roy, Mat. Res. Bull. **19**, 471 (1984).
[2]D. K. Agrawal and V. S. Stubican, Mat. Res. Bull. **20**, 99 (1985).
[3]R. M. Hazen, L. W. Finger, D. K. Agrawal, H. A. McKinstry, and A. J. Perrotta, J. Mat. Res. **2**, 329 (1987).
[4]L. Hagman and P. Kierkegaard, Acta Chemica Scand. **22**, 1822 (1968).
[5]N. G. Chernorukov, I. A. Korshunov, and T. V. Prokof'eva, Kristallografiya **23**, 884 (1978) [Sov. Phys.—Crystallog. **243**, 475 (1978)].
[6]J. B. Goodenough, H. Y.-P. Hone, and J. A. Kafalas, Mat. Res. Bull. **11**, 173 (1976).
[7]S. Y. Limaye, D. K. Agrawal, and H. A. McKinstry, J. Am. Ceram. Soc. **70**, C232 (1987).
[8]See, for an example of applying the model to ferroelectric perovskites, G. Schäfer, P. J. Herzog, and B. Wolbeck, Z. Phys. **257**, 336 (1972), or, for an example of applying the model to a semiconductor, K. Krusch and J. A. Gardner, Phys. Rev. B **24**, 4587 (1981).
[9]See, for example, R. Bauer, C. Christensen, and E. Larsen, J. Chem. Phys. **70**, 4117 (1979).
[10]For a review see, E. Recknagel and T. Wichert, Nucl. Instrum. Methods **182/183**, 439 (1981).

[11]See, for example, C. Allard, G. S. Collins, and C. Hohenemser, Phys. Rev. B **32**, 4839 (1985).
[12]M. L. Swanson, T. Wichert, and A. F. Quenneville, Appl. Phys. Lett. **49**, 265 (1986).
[13]T. P. Das and P. C. Schmidt, Z. Naturforsch., Teil A **41**, 47 (1986).
[14]E. N. Kaufmann and R. J. Vianden, Rev. Mod. Phys. **51**, 161 (1979).
[15]K. W. Lodge and C. A. Sholl, J. Phys. F **4**, 2073 (1974).
[16]K. Nishiyama and D. Riegel, Phys. Lett. **57A**, 270 (1976).
[17]K. Nishiyama, F. Dimmling, T. Kornrumpf, and D. Riegel, Phys. Rev. Lett. **37**, 357 (1976).
[18]K. Nishiyama, F. Dimmling, T. Kornrumpf, and D. Riegel, Phys. Lett. **62A**, 247 (1977).
[19]M. D. Thompson, P. C. Pattnaik, and T. P. Das, Hyp. Interact. **4**, 515 (1978).
[20]K. Nishiyama and D. Riegel, Hyp. Interact. **4**, 490 (1978).
[21]E. Bodenstedt, B. Persheid, and S. Nagel, Z. Phys. B **63**, 9 (1986).
[22]M. Frank, F. Gubitz, W. Ittner, W. Kreische, A. Labahn, B. Röselen, and G. Weeske, Z. Naturforsch., Teil. A **41**, 104 (1986).
[23]K. Krusch and J. A. Gardner, Phys. Rev. B **26**, 3973 (1982).
[24]L. Amaral, M. Behar, A. Maciel, and H. Saitovitch, Phys. Lett. **102A**, 45 (1984).
[25]M. Behar, E. R. Fraga, A. Maciel, W. H. Schreiner, and H. Saitovitch, J. Phys. C **18**, 5863 (1985).
[26]T. Butz, A. Hübler, and A. Lerf, Phys. Rev. B **26**, 3973 (1982).
[27]M. M. Hafiz, M. M. Ibrahim, and A. S. Ahmed, Phys. Status Solidi A **71**, 259 (1982).
[28]For a review, see W. Witthuhn, Hyp. Interact. **24**, 547 (1985).
[29]H. Barfusz, G. Böhnlein, H. Hohenstein, W. Kreische, N. Niedrig, H. Appel, R. Heidringer, J. Randies, G. Then, and W. G. Thies, Z. Phys. **47**, 99 (1982).
[30]H. Jaeger, J. A. Gardner, J. C. Haygarth, and R. L. Rasera, J. Am. Ceram. Soc. **69**, 458 (1986).
[31]M. C. Caracoche, A. R. López García, J. A. Martínez, L. A. Mendoza Zelis, and R. C. Mercader, Phys. Rev. B **25**, 5972 (1982).
[32]J. A. Martínez, P. C. Rivas, M. C. Caracoche, A. M. Rodríguez, and A. R. López García, Hyp. Interact. **30**, 9 (1986).
[33]M. T. Dova, P. C. Rivas, J. A. Martínez, M. C. Caracoche, and A. R. López García, Hyp. Interact. **30**, 199 (1986).
[34]P. C. Rivas, M. C. Caracoche, J. A. Martínez, M. T. Dova, and A. R. López García, Hyp. Interact. **30**, 49 (1986).
[35]A. M. Rodríguez, M. C. Caracoche, J. A. Martínez, and A. R. López García, Hyp. Interact. **30**, 277 (1986).
[36]H. Frauenfelder and R. Steffen, *Angular Distribution of Nuclear Radiation in Alpha-, Beta-, and Gamma-Ray Spectroscopy,* edited by K. Siegbahn (North-Holland, Amsterdam, 1965), Vol. 2, pp. 997–1196.
[37]A. Abragam and R. Pound, Phys. Rev. **92**, 943 (1953).
[38]E. Gerdau, J. Wolf, H. Winkler, and J. Braunsfurth, Proc. R. Soc. London, Ser. A **311**, 197 91969).
[39]H. Winkler and E. Gerdau, Z. Phys. **262**, 363 (1973).
[40]M. Blume, Nucl. Phys. A **167**, 81 (1971).
[41]F. Bosch and H. Spehl, Z. Phys. **268**, 145 (1974).
[42]A. R. Gallant, Am. Stat. **29**, 73 (1973).
[43]The magnitudes of the conductivity measurements are not absolute. They may depend on many microstructural factors such as the density and the grain morphology as well as the presence of a second phase (which in this case was not observed). Also, the magnitude of the conductivity depends on the ratio of the sample thickness to the electrode surface area. This ratio was taken from the geometrical measurement which may not reflect the actual current path. For the purpose of the analysis, we assume that these systematic effects do not change with temperature.
[44]J. W. Ball and M. Kaplan, J. Chem. Phys. **69**, 117 (1978).
[45]M. H. Cohen and F. Reif, *Solid State Physics,* edited by F. Seitz and D. Turnbull (Academic, New York, 1975), Vol. 5, pp. 321–438.
[46]F. D. Feiock and W. R. Johnson, Phys. Rev. **187**, 39 (1969).
[47]A. J. Nozik and M. Kaplan, Phys. Rev. **159**, 273 (1967).
[48]H. Kohler, H. Schulz, and O. Melnikov, Mat. Res. Bull. **18**, 1143 (1983).
[49]R. J. Cava, E. L. Vogel, and D. W. Johnson, J. Am. Ceram. Soc. **65**, C157 (1982).
[50]U. Von Alpen and M. F. Bell, *Sodium Ion Conductors—NASICON and Na β-Alumina,* Proceedings of the International Conference on Fast Ion Transport in Solids, May, 1979, edited by P. Vashita, J. Mundy, and G. Shenoy (Elsevier, Amsterdam, 1979), pp. 443–446.
[51]M. Zahir, R. Olazcuaga, and P. Hagenmuller, Mater. Lett. **2**, 234 (1984).
[52]M. L. Bayard and G. G. Barna, J. Electroanal. Chem. **91**, 201 (1978).
[53]D. Petit, P. Colomban, G. Collin, and J. P. Boilot, Mat. Res. Bull. **21**, 365 (1986).
[54]D. Tran Qui, J. J. Capponi, and J. C. Joubert, J. Solid State Chem. **39**, 219 (1981).
[55]C. L. Tsai and H. Hong, Mat. Res. Bull. **18**, 1399 (1983).
[56]G. Desplanches, M. Rigal, and A. Wicker, Ceram. Bull. **59**, 546 (1980).
[57]J. P. Boilot, J. P. Salanie, G. Desplanches, and D. Le Potier, Mat. Res. Bull. **14**, 1469 (1979).
[58]A. Baudry, P. Boyer, A. L. De Oliveiro, J. Phys. Chem. Solids **43**, 871 (1982).
[59]R. S. Raghavan, E. N. Kaufman, and P. Raghavan, Phys. Rev. Lett. **34**, 1280 (1975).
[60]J. M. Ziman, *Principles of the Theory of Solids,* 2nd ed. (Cambridge University Press, New York, 1972), pp. 62-64.
[61]D. K. Agrawal (unpublished).